Intranight optical variability of blazars and radio-quiet quasars using the ZTF survey

Vibhore Negi [1,2]★ Gopal-Krishna,[3] Ravi Joshi [4,5] Hum Chand,[6] Paul J. Wiita,[7] P. K. Navaneeth[8] and Ravi S. Singh[2]

[1]*Aryabhatta Research Institute of Observational Sciences (ARIES), Manora Peak, Nainital 263002, Uttarakhand, India*

[2]*Department of Physics, Deen Dayal Upadhyaya Gorakhpur University, Gorakhpur 273009, Uttar Pradesh, India*

[3]*UM-DAE Centre for Excellence in Basic Sciences, Vidyanagari, Mumbai 400098, Maharashtra, India*

[4]*Indian Institute of Astrophysics, Koramangla, Bengaluru 560034, Karnataka, India*

[5]*Kavli Institute for Astronomy and Astrophysics, Peking University, Beijing 100871, China*

[6]*Department of Physics and Astronomical Science, Central University of Himachal Pradesh (CUHP), Dharamshala 176215, Himachal Pradesh, India*

[7]*Department of Physics, The College of New Jersey, PO Box 7718, Ewing, NJ 08628-0718, USA*

[8]*Department of Physics, Central University of Karnataka, Kadaganchi 585367, Karnataka, India*

ABSTRACT

We explore the potential of the ongoing Zwicky Transient Facility (ZTF) survey for studying intranight optical variability (INOV) of active galactic nuclei (AGNs), in particular for picking rare events of large INOV amplitudes, whose detection may require extensive temporal coverage. For this, we have used the available high cadence subsets of the ZTF data base to build a well-defined large sample of 53 blazars and another sample of 132 radio-quiet quasars (RQQs), matched to the blazar sample in the redshift−magnitude plane. High-cadence ZTF monitoring of these two matched samples is available, respectively, for 156 and 418 intranight sessions. Median durations for both sets of sessions are 3.7 h. The two classes of powerful AGNs monitored in these sessions represent opposite extremes of jet activity. The present analysis of their ZTF light curves has revealed some strong INOV events that, although not exceptionally rare for blazars, are indeed so for RQQs, and their possible nature is briefly discussed.

Key words: galaxies: active – BL Lacertae objects: general – galaxies: jets – galaxies: photometry – quasars: general.

1 INTRODUCTION

Active galactic nuclei (AGNs) are known to radiate over a very wide frequency range, from radio to TeV γ-rays, and to show flux variability across the electromagnetic spectrum on diverse time-scales (Blandford & Rees 1978; Urry & Padovani 1995; Wagner & Witzel 1995; Ulrich, Maraschi & Urry 1997). This characteristic has been extensively used to probe the physics of their central engines that remain spatially unresolved in direct observations (e.g. reviews by Antonucci 1993; Marscher 2016; Blandford, Meier & Readhead 2019). The optical flux variations of AGNs on hour-like (or even shorter) time-scales are commonly referred to as 'micro-variability' (Miller, Carini & Goodrich 1989) or 'intranight optical variability' (INOV; Gopal-Krishna, Sagar & Wiita 1995; Gopal-Krishna et al. 2003). In the case of blazars and other γ-ray-detected AGNs, INOV amplitude (ψ) reaching a tenth of magnitude, or even more, is not very rare, whereas much weaker INOV is displayed by the remaining classes of AGN (e.g. Stalin et al. 2004a, b; Goyal et al. 2013; Gopal-Krishna & Wiita 2018, hereafter GW18).

The INOV of blazars is widely linked to turbulence in their relativistic jets (e.g. Marscher, Gear & Travis 1992; Goyal et al. 2012; Marscher 2014; Calafut & Wiita 2015; Webb et al. 2021), such that any tiny emissivity fluctuations arising within the jet flow can appear hugely amplified due to the jet's bulk relativistic motion (e.g. Singal & Gopal-Krishna 1985; Giannios, Uzdensky & Begelman 2009; Biteau & Giebels 2012; Narayan & Piran 2012). It has been suggested that a broadly similar but milder version of this process, occurring inside intrinsically weak and less well aligned relativistic jet, could account for the low-level INOV exhibited by radio-quiet quasars (RQQs) (Gopal-Krishna et al. 2003, hereafter GSSW03; Stalin et al. 2004b). On the other hand, INOV of RQQs could even arise from flares occurring in the magnetized plasma of the accretion disc and in its environment (Zhang & Bao 1991; Mangalam & Wiita 1993) or due to shocks/instabilities in the accretion disc (Chakrabarti & Wiita 1993). Such possibilities make INOV studies a useful probe of the physics of the central engine and the relativistic jets emanating from it.

Although a good deal of observational effort has been invested over the past few decades, on characterizing the INOV displayed by diverse classes of AGN, the focus in most campaigns has clearly been on blazars (e.g. see the reviews GW18; Gupta 2018; Webb 2021). In such studies, each AGN was typically monitored quasi-continuously for durations between 2 and 6 h, using 1–2 m-class optical telescopes, thus achieving an INOV detection limit of $\sim$1–2 per cent of amplitude (ψ). A large duty cycle of INOV detection (DC $\sim$50–70 per cent)

★ E-mail: vibhore@aries.res.in, vibhore.negi18@gmail.com

has thus been established for BL Lacertae objects (BL Lacs) and the flat-spectrum radio quasars (FSRQs) exhibiting a high fractional polarization ($p_{opt} > 3$ per cent). In contrast, the remaining AGN classes, even including low-polarization FSRQs whose nuclear radio jets are relativistically beamed towards us, and the lobe-dominated radio quasars, were all found to exhibit only mild INOV (typically, $\psi \lesssim 3$ per cent), with a small INOV DC of approximately 10 per cent (see e.g. GSSW03 and references therein; Romero et al. 2002; Stalin et al. 2004a; Goyal et al. 2013; GW18).

In this work, we report a search for high-amplitude INOV of blazars and RQQs, the two classes of powerful AGN that represent the opposite extremes in jet activity. As compared to their previous INOV studies, our present samples of these two AGN classes are significantly larger and have been monitored more extensively, as part of the Zwicky Transient Facility (ZTF) survey (Masci et al. 2019), without any consideration of the activity levels of the individual sources. The ZTF survey scans the northern sky using a 47-deg^2 wide-field imager mounted on a 48-inch Schmidt telescope on Mount Palomar. The data base provides long-term light curves (LCs) interspersed with high cadence LCs that can be used for detecting rare events of large INOV. We first describe in Section 2 our sample selection and the ancillary data used. Section 3 describes the data analysis and presents the results obtained. This is followed by a brief discussion in Section 4. Our main conclusions are summarized in Section 5.

2 THE DATA AND SAMPLE SELECTION

The parent catalogue of the blazars covered in this study is the ROMA-BZCAT (Massaro et al. 2015), which lists a total of 3561 blazars, classified as BL Lacs, or FSRQs. Only 2751 of them were found in the ZTF data base (ZTF DR10[1]). Out of these, we discarded 159 blazars labelled as 'uncertain type' and another 71 as 'candidate' BL Lac in the ROMA-BZCAT. Next, since the surface-brightness profile of the host galaxy of an AGN does not generally behave like a point source when convolved with the 'point spread function' (PSF), any intranight variation in PSF (i.e. 'seeing') can give rise to a changing ratio of light contributions from the AGN and its host galaxy. Such LCs can lead to spurious claims of INOV (Carini et al. 1991; Cellone, Romero & Combi 2000). In order to reduce this possibility to a negligible level, we have only selected sources lying at redshifts $z > 0.3$, leaving us with 1555 sources. Their (PSF-fitting-based) r-band LCs available in the ZTF data base were firstly cleaned up by accepting only the 'good quality' data, i.e. discarding the data points with ZTF CATFLAG score of zero. The ZTF survey determines model PSFs and employs them to generate a PSF-fit photometry catalogue using a version of DAOPHOT (Stetson 1987) optimized for ZTF, including an added benefit of de-blending by fitting to multiple detections simultaneously in a two-pass PSF fit (Masci et al. 2019). Further, ZTF treats the LCs observed in a particular field, filter, and CCD quadrant independently, and assigns them different observation IDs. Since combining the LCs from different fields and CCD quadrants can induce spurious variability, we have accepted for a given source only the LC corresponding to the observation ID with the highest number of data points (see also Negi et al. 2022). Next, in order to reduce the number of LCs with poor signal-to-noise ratio, we rejected all the sources having mean $m_r > 19$ over the duration of the ZTF survey.

As further filters, we rejected the LCs of duration (T) < 2 h and also those having gap(s) of > 1 h. As ZTF employs a small telescope (48-inch) and the exposure time for a single frame is small ($\sim$30 s), the photometric errors are relatively large for fainter sources. Hence, we have carried out a three-point median binning of the LCs, when required, provided the binning does not reduce the number (N) of data points in an LC to below 10. Thereafter, in order to reduce noisy LCs, we rejected sessions for which average quoted photometric error of the data points is >0.03 mag.

Lastly, as our final filter, all remaining sessions with less than 10 data points were discarded, leaving us with a final sample of 53 blazars, monitored in 156 ZTF intranight sessions. These consist of 46 FSRQs (138 sessions) and 7 BL Lacs (18 sessions). For comparing the INOV of this sample of blazars with that of RQQs, we then constructed a preliminary 'matched sample' of RQQs out of the SDSS DR14 (Pâris et al. 2018). The matching was done in the z–m_r plane, setting tolerances of ± 0.1 and ± 0.2 mag, respectively. This resulted in a set of about 20 matched RQQs for each blazar. For the matched sample of RQQs, we checked for the availability of ZTF r-band LCs and the same were found for 132 of the RQQs (418 sessions). Kolmogorov–Smirnov test (KS-test) on the two matched samples provides a D-statistic of 0.18 for magnitude and 0.09 for redshift, with a probability of null hypothesis being 0.14 and 0.91, respectively (see Fig. 1). Details of the blazar sample and the matched RQQ sample are given in Tables A1 and A2. The median durations (T) of the LCs are found to be 3.7 h for both the blazar sample and the matched RQQ sample, with $\sim$75 per cent of the blazar sessions and $\sim$84 per cent of the RQQ sessions having $T > 3$ h (up to $\sim$4 h; see Fig. 2).

3 ANALYSIS AND RESULTS

A preliminary check for INOV in the ZTF LCs (which are based on PSF-fitting photometry) of our matched samples of 53 blazars (156 sessions) and 153 RQQs (418 sessions) was made employing the widely used F-test (de Diego 2010). The F-value for each LC was computed from

$$F = \frac{\text{Var}(q)}{\sum_{i=1}^{N} \sigma_{i,\text{err}}^2(q)/N},\tag{1}$$

where $\text{Var}(q)$ is the variance of the LC of the target AGN (RQQ/blazar), $\sigma_{i,\text{err}}(q)$ is the rms error on the i-th data point in the LC of the target AGN, and N is the number of data points in the LC. The computed value of F for each LC was compared with the critical F-value (F_c) computed for that session, for 99 per cent confidence level. The LCs showing $F \geq F_c$ (0.99) were shortlisted as candidates for INOV detection. In the next level check, each candidate LC was subjected to visual inspection of the optical field around both the target AGN and 3–4 comparison stars monitored concurrently with the AGN on the same CCD chip. The comparison stars were selected applying the criteria of a clean optical neighbourhood (the criterion also employed for the AGN, before claiming its INOV detection), as well as proximity to the target AGN in both position (within $\sim$5 arcmin) and m_r ($|\Delta m_r| \lesssim 1.0$). The LCs of the comparison stars were then subjected to the F-test mentioned above. Applying this procedure, which is equivalent to the widely practiced 'differential photometry', to the shortlisted LCs of both the target AGN and the comparison stars, we were able to isolate good INOV candidate LCs of the blazars and RQQs [for which the computed $F > F_c(0.99)$, unlike the set of comparison stars]. All these LCs were subjected to a final check for any systematic variation in PSF (obtained from the ZTF data base) during the respective monitoring session and
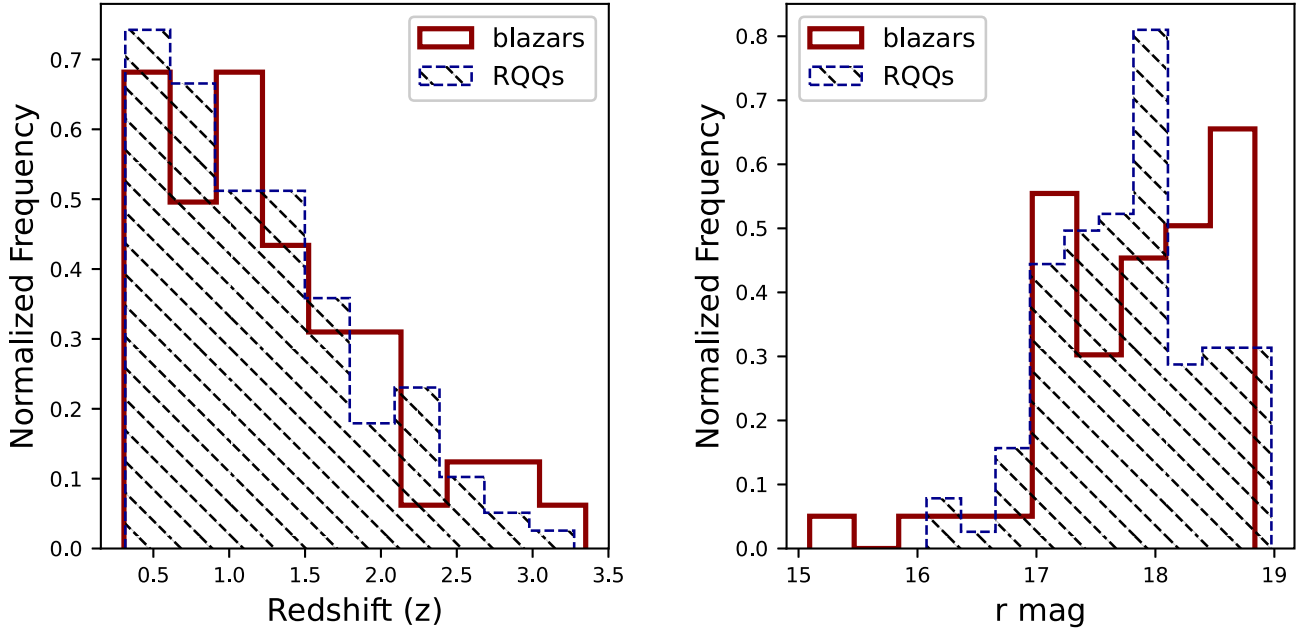
Figure 1. The redshift and apparent magnitude distributions of the sample of blazars (53) and the control sample of RQQs (132). Left-hand panel: Median values of redshift for the two distributions are 1.15 (blazars) and 1.07 (RQQs). Right-hand panel: Distribution of the *r*-band apparent magnitudes for the blazar and RQQ samples, having median values of 18.0 and 17.8 mag, respectively.
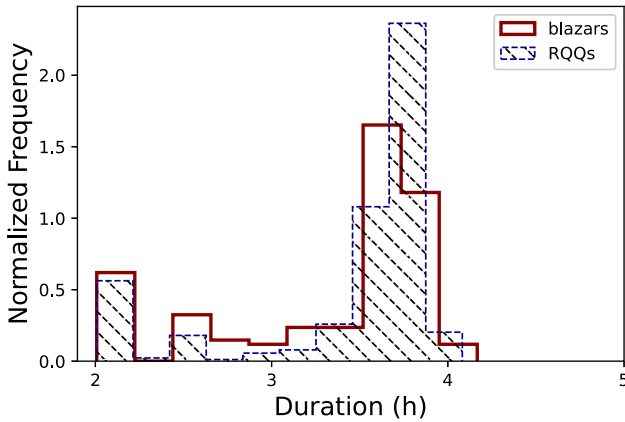
Figure 2. The distributions of the observed time duration (T) for the LCs of blazars (156) and RQQs (418). The median values for both histograms are 3.7 h.

any AGN LC showing a variability trend correlated with the PSF variation was deemed to be unreliable and discarded. The above sequence of reliability checks has led to confirmation of INOV for six blazar sessions (involving four blazars) and three RQQ sessions.

Table 1 lists the computed *F*-values for all these nine LCs found to exhibit INOV in our analysis, along with the critical *F*-values at the desired significance level of α ($= F_c^\alpha$). All these nine AGN LCs, together with the LCs of the corresponding comparison stars, are displayed in Figs 3–4, together with the respective PSF variation profiles. The images of the optical fields are shown in Figs A1 and A2. Also provided with each AGN LC are several observational and computed parameters, including the *F*-values (equation 1) and the INOV amplitude (ψ) that has been computed from the relation (Heidt

& Wagner 1998)

$$\psi = \sqrt{(A_{max} - A_{min})^2 - 2\sigma^2},\qquad(2)$$

where A_{max} and A_{min} are the maximum and minimum values of the AGN LC and $\sigma^2 = <\sigma_q^2>$, where σ_q is the mean rms error for the data points in the LC.

4 DISCUSSION

The small number of the INOV events confirmed here in the ZTF LCs of the matched samples of blazars and RQQs can probably be ascribed to a combination of (i) the modest photometric sensitivity, specially for the large fraction of objects in our sample that are relatively faint ($m_r > 17.5$), and (ii) the short durations (T) of the LCs (median $\sim$3.7 h, Fig. 2).[2] Since the duration of nearly all our LCs is under 4 h, it is likely that the number of INOV detections has been underestimated for this reason. Furthermore, a good fraction of the blazars in the sample, although having a flat radio spectrum, may well be lacking a high optical polarization, which is a crucial diagnostic for INOV detection, as shown by Goyal et al. (2012). None the less, the small number of INOV events does not detract from the basic objective of our study, which is to look for any exceptionally large, rare INOV events, taking advantage of the extraordinarily large temporal coverage afforded by the ZTF data base. Such an INOV search is particularly salient for RQQs, as compared to blazars for which an extensive INOV literature has accumulated over the past three decades.

For the blazars, $\psi > 10$ per cent stands confirmed in four sessions, which is not unfamiliar (see e.g. the surveys by Heidt &

---

[2]It is known that the probability of INOV detection increases with the monitoring duration (T), at least up to 5–6 h (e.g. Gupta & Joshi 2005; Carini et al. 2007).

Table 1. Results of INOV analysis for the blazars (BLs) and RQQs in our sample, showing INOV detection.

AGNs	Date of Obs.	N	T	F-test		$\overline{\psi}$
	yyyy/mm/dd		(h)	$F_c(0.99)$	F_{LC}	(per cent)
(1)	(2)	(3)	(4)	(5)	(6)	(7)
BL J064828.5−174405	2018-12-12	46	2.96	2.02	3.27	9
BL J071355.7+193500	2019-11-08	68	2.18	1.78	1.94	19
BL J071355.7+193500	2019-12-18	14	2.53	3.91	21.61	28
BL J071355.7+193500	2019-12-19	19	3.90	3.13	23.99	35
BL J074836.1+240024	2020-01-01	18	3.88	3.24	5.54	9
BL J081126.7+014652	2020-01-04	19	3.63	3.13	5.12	8
RQQ J082443.8+201901	2019-11-08	68	2.18	1.78	1.81	13
RQQ J085903.6+123903	2019-11-26	59	2.06	1.86	5.84	14
RQQ J092727.4-020832	2019-02-12	18	3.59	3.24	3.80	15
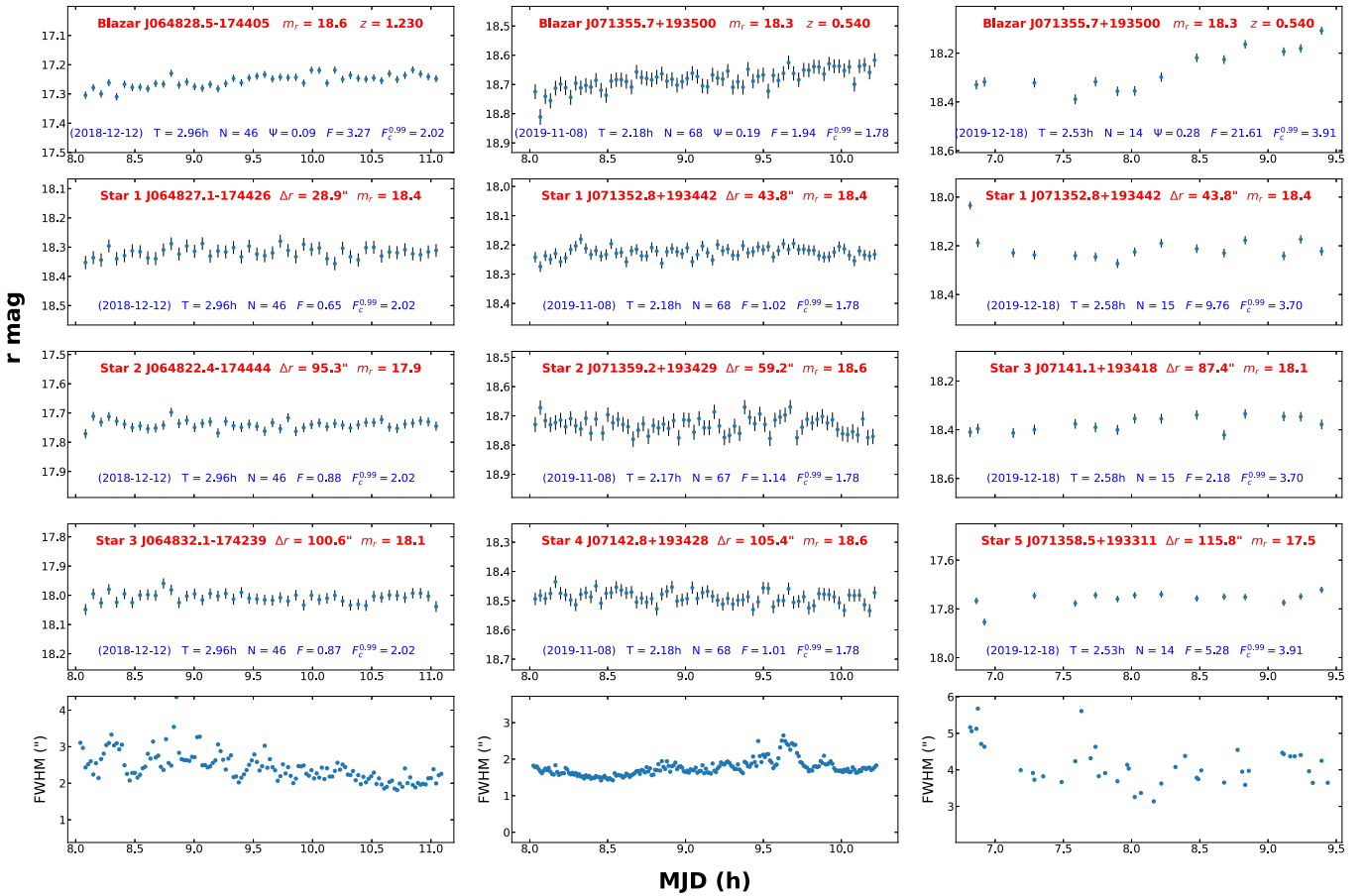
Figure 3. The LCs of the blazar sessions with INOV confirmed in the present analysis. For each session, the top panel shows the LC of the target blazar, and the subsequent three lower panels show the LCs of the three selected comparison stars, in order of increasing distance (Δr) from the blazar. For each blazar/star, basic properties are mentioned near the top in the panel, whereas the estimated parameters from the variability analysis of the session are displayed near the bottom of the panel. The lowest panel shows the variation of the seeing (PSF) through the monitoring session.

Wagner 1998; Romero, Cellone & Combi 1999; Sagar et al. 2004; Stalin et al. 2004b; Webb et al. 2021). On the other hand, INOV events of such large amplitudes are exceptional in the case of RQQs, considering their much more modest INOV levels reported in the literature so far (Gopal-Krishna, Sagar & Wiita 1993, 1995; Jang & Miller 1995, 1997; Romero et al. 1999; Gopal-Krishna et al. 2003; Ramírez et al. 2004, 2009; Stalin et al. 2004a; Gupta & Joshi 2005; Carini et al. 2007; Joshi et al. 2011; Goyal et al. 2012; Joshi

& Chand 2013). These studies have led to an upper limit of ψ = 3–5 per cent for RQQs (GW18). This work has revealed three INOV sessions for RQQs with ψ > 10 per cent (up to 15 per cent; see Fig. 4). These are J082443.8+201901, J085903.6+123903, and J092727.4−020832 (Table 1 and Fig. 4). We note that all these quasars are undetected in the Very Large Array Sky Survey (VLASS) at 3 GHz and we have adopted an upper limit of 384 μJy for each of them, being 3 rms noise for the survey (Gordon et al. 2021). The
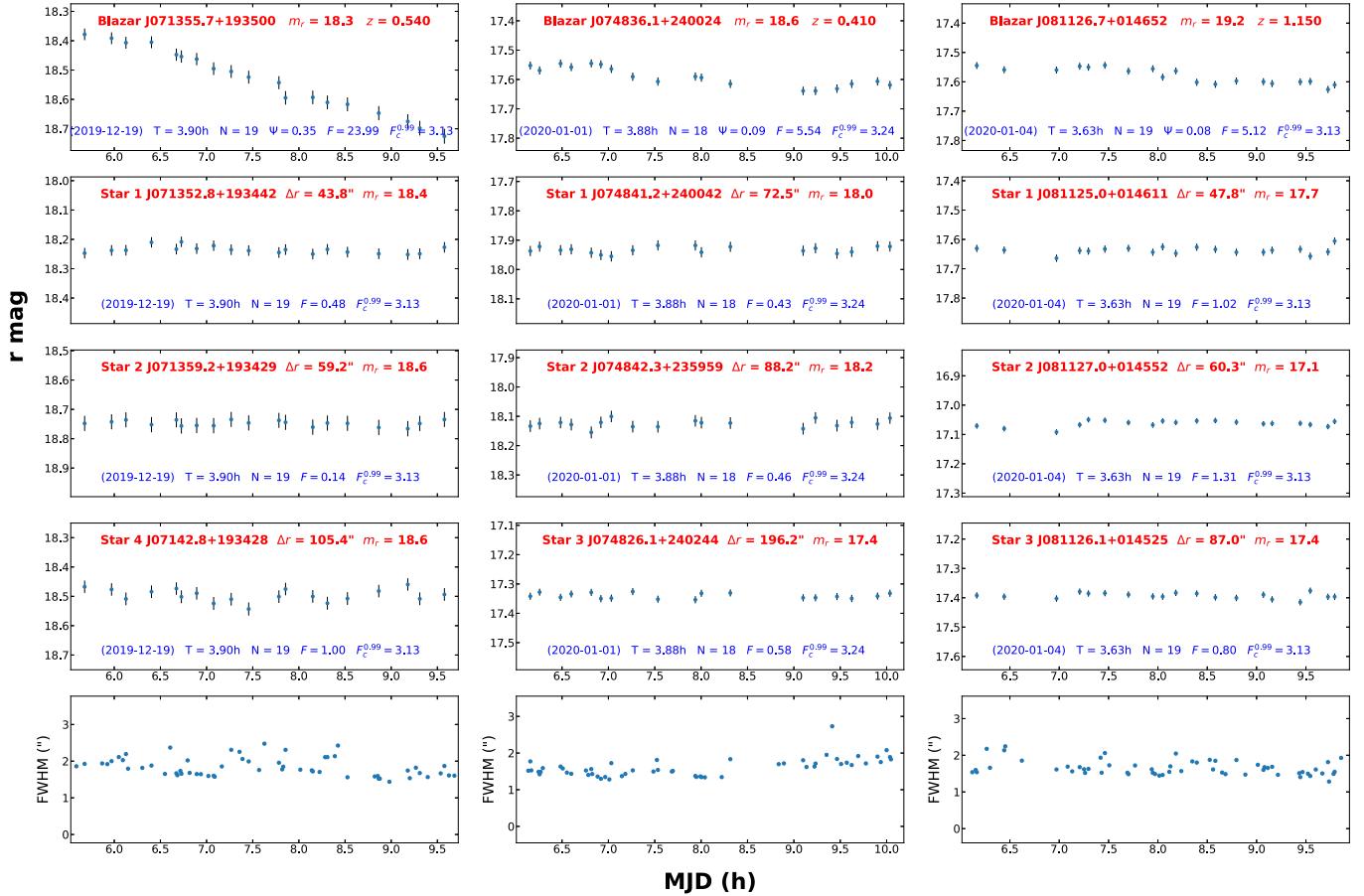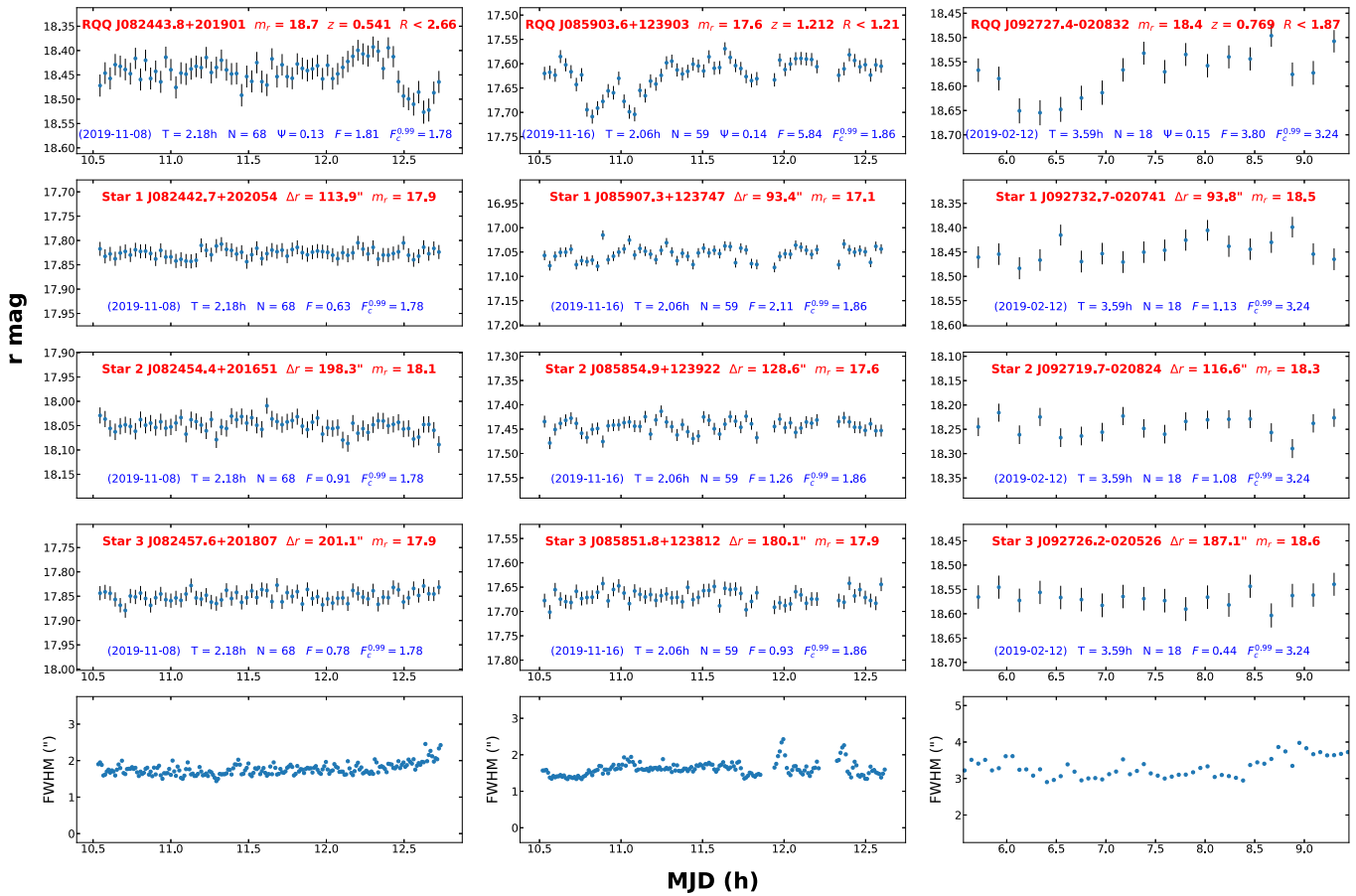
Figure 3 – *continued*

corresponding upper limits for the radio-loudness parameter R_{5GHz} are 2.7, 1.2, and 1.9, respectively, i.e. below the threshold R = 10 (Kellermann et al. 1989).[3] Thus, we find here that even RQQs can, in rare instances, exhibit INOV amplitudes at levels that had hitherto been recorded only for radio-loud AGNs of blazar type. It is also interesting to note that in two of the three sessions (2019-11-08 and 2019-11-16, Fig. 4), the observed INOV is a dip in the LC. These temporally well-resolved emission dips on time-scale of ∼1 h are similar to the striking 4 per cent amplitude dip of 1-h duration, which occurred during the intranight optical monitoring of the TeV blazar PG1553+113 (Gopal-Krishna et al. 2011). Those authors interpreted the short-duration dip in terms of a dusty cloud in the foreground of a superluminal optical knot in the jet, consistent with the scenario of 'superluminal gravitational lensing' proposed for blazar variability (Gopal-Krishna & Subramanian 1991). This explanation invoking foreground dusty cloud(s) would also be in accord with the fact that PG 1553+111 is known to have the highest known rotation

measure among TeV blazars (Lico et al. 2020). However, if such an explanation were also to be applicable for the emission dips found here in the LCs of the two RQQs (Fig. 4), these RQQs would also be required to have superluminal optical jets (or micro-jets) in their nuclei. Thus, even in the event that their observed INOV has an external origin (and not directly originating within a relativistic jet, unlike the INOV of blazars), the present INOV observations of the two RQQs would still require the presence of a relativistic micro-jet in the nucleus. Various arguments and literature supporting such a possibility are summarized, e.g. in Hartley et al. (2019).

5 CONCLUSIONS

This study underscores the potential of the ongoing ZTF survey for detecting rare events of strong INOV of AGNs, particularly among RQQs whose INOV is generally known to be mild (no more than a few per cent). To search for stronger INOV levels, we have made use of ZTF data base for a well-defined sample of 53 blazars (156 sessions) and a matched sample containing 132 RQQs (418 sessions). INOV was thus detected in six and three ZTF sessions, targeting the blazar and RQQ samples, respectively. In these sessions, INOV amplitudes $\psi > 10$ per cent were detected not only for the six blazar sessions (which is not exceptional) but, unexpectedly, also in three RQQ sessions. This shows that a blazar-like INOV level can also be attained by RQQs, albeit very rarely. Note that two of these three INOV events are in fact well-resolved brightness 'dips' (∼14 per cent), lasting about 1 h or less. An analogy with a similar well-

---

[3]The radio-loudness parameter has been estimated as R $= F_{5GHz}/F_B$. Due to non-detection of the targets at radio bands, radio flux (F_{5GHz}) has been estimated assuming the flux at 3 GHz to be $< 384 \mu$Jy (i.e. 3σ limit of the VLASS survey at 3 GHz; see Gordon et al. 2021) and scaling it to 5 GHz, using a spectral index (α) of -0.7. The flux at B-band (F_B) has been estimated from the apparent magnitude B taken from SIMBAD, using relation given by Schmidt & Green (1983). Due to the non-availability of m_B for the RQQ J092727.4−020832, its B-mag has been estimated from u and g magnitudes, using the transformation equations given by Jester et al. (2005).

Figure 4. The LCs of the three RQQ sessions with INOV confirmed in the present analysis. The top panel shows the LC of the RQQ and the subsequent three lower panels show the LCs of three comparison stars in the order of increasing distance (Δr) from the RQQ. For each RQQ/star, the basic properties are given near the top of the panel, whereas the estimated parameters from the variability analysis for the session are displayed near the bottom of the panel. The lowest panel shows the variation of the seeing (PSF) through the monitoring session.

resolved dip lasting $\sim$1 h, observed in an LC of the TeV blazar PG 1553+111, suggests that the nuclei of these two RQQs probably also contain micro-jets of optical emission performing bulk relativistic motion.

This research has made use of the NASA/IPAC Extragalactic Data base (NED), which is operated by the Jet Propulsion Laboratory, California Institute of Technology, under contract with the National Aeronautics and Space Administration.

DATA AVAILABILITY

The data used in this study are publicly available in the ZTF DR10.

REFERENCES

Abdo A. A. et al., 2010, ApJ, 716, 30
Antonucci R., 1993, ARA&A, 31, 473
Biteau J., Giebels B., 2012, A&A, 548, A123
Blandford R. D., Rees M. J., 1978, in Wolfe A. M., ed., Pittsburgh Conf. on BL Lac Objects. Univ. Pittsburgh, Pittsburgh, PA, p. 328
Blandford R., Meier D., Readhead A., 2019, ARA&A, 57, 467
Calafut V., Wiita P. J., 2015, J. Astrophys. Astron., 36, 255
Carini M. T., Miller H. R., Noble J. C., Sadun A. C., 1991, AJ, 101, 1196
Carini M. T., Noble J. C., Taylor R., Culler R., 2007, AJ, 133, 303
Cellone S. A., Romero G. E., Combi J. A., 2000, AJ, 119, 1534
Chakrabarti S. K., Wiita P. J., 1993, ApJ, 411, 602
Chambers K. C. et al., 2016, preprint (arXiv:1612.05560)
de Diego J. A., 2010, AJ, 139, 1269
Giannios D., Uzdensky D. A., Begelman M. C., 2009, MNRAS, 395, L29

Gopal-Krishna, Subramanian K., 1991, Nature, 349, 766
Gopal-Krishna, Wiita P. J., 2018, Bull. Soc. R. Sci. Liege, 87, 281 (GW18)
Gopal-Krishna, Sagar R., Wiita P. J., 1993, MNRAS, 262, 963
Gopal-Krishna, Sagar R., Wiita P. J., 1995, MNRAS, 274, 701
Gopal-Krishna, Stalin C. S., Sagar R., Wiita P. J., 2003, ApJ, 586, L25 (GSSW03)
Gopal-Krishna, Goyal A., Joshi S., Karthick C., Sagar R., Wiita P. J., Anupama G. C., Sahu D. K., 2011, MNRAS, 416, 101
Gordon Y. A. et al., 2021, ApJS, 255, 30
Goyal A., Gopal-Krishna, Wiita P. J., Anupama G. C., Sahu D. K., Sagar R., Joshi S., 2012, A&A, 544, A37
Goyal A., Gopal-Krishna, Wiita P. J., Stalin C. S., Sagar R., 2013, MNRAS, 435, 1300
Gupta A., 2018, Galaxies, 6, 1
Gupta A. C., Joshi U. C., 2005, A&A, 440, 855
Hartley P., Jackson N., Sluse D., Stacey H. R., Vives-Arias H., 2019, MNRAS, 485, 3009
Heidt J., Wagner S. J., 1998, A&A, 329, 853
Jang M., Miller H. R., 1995, ApJ, 452, 582
Jang M., Miller H. R., 1997, AJ, 114, 565
Jester S. et al., 2005, AJ, 130, 873
Joshi R., Chand H., 2013, MNRAS, 429, 1717
Joshi R., Chand H., Gupta A. C., Wiita P. J., 2011, MNRAS, 412, 2717
Kellermann K. I., Sramek R., Schmidt M., Shaffer D. B., Green R., 1989, AJ, 98, 1195
Lico R. et al., 2020, A&A, 634, A87
Mangalam A. V., Wiita P. J., 1993, ApJ, 406, 420
Marscher A. P., 2014, ApJ, 780, 87
Marscher A., 2016, Galaxies, 4, 37
Marscher A. P., Gear W. K., Travis J. P., 1992, in Valtaoja E., Valtonen M., eds, Variability of Blazars. Cambridge Univ. Press, Cambridge, New York, p. 85

Masci F. J. et al., 2019, PASP, 131, 018003
Massaro E., Maselli A., Leto C., Marchegiani P., Perri M., Giommi P., Piranomonte S., 2015, Ap&SS, 357, 75
Miller H. R., Carini M. T., Goodrich B. D., 1989, Nature, 337, 627
Narayan R., Piran T., 2012, MNRAS, 420, 604
Negi V., Joshi R., Chand K., Chand H., Wiita P., Ho L. C., Singh R. S., 2022, MNRAS, 510, 1791
Pâris I. et al., 2018, A&A, 613, A51
Ramírez A., de Diego J. A., Dultzin-Hacyan D., González-Pérez J. N., 2004, A&A, 421, 83
Ramírez A., de Diego J. A., Dultzin D., González-Pérez J. N., 2009, AJ, 138, 991
Romero G. E., Cellone S. A., Combi J. A., 1999, A&AS, 135, 477
Romero G. E., Cellone S. A., Combi J. A., Andruchow I., 2002, A&A, 390, 431
Sagar R., Stalin C. S., Gopal-Krishna, Wiita P. J., 2004, MNRAS, 348, 176
Schmidt M., Green R. F., 1983, ApJ, 269, 352
Singal K. A., Gopal-Krishna, 1985, MNRAS, 215, 383
Stalin C. S., Gopal-Krishna, Sagar R., Wiita P. J., 2004a, J. Astrophys. Astron., 25, 1
Stalin C. S., Gopal-Krishna, Sagar R., Wiita P. J., 2004b, MNRAS, 350, 175
Stetson P. B., 1987, PASP, 99, 191
Ulrich M.-H., Maraschi L., Urry C. M., 1997, ARA&A, 35, 445
Urry C. M., Padovani P., 1995, PASP, 107, 803
Wagner S. J., Witzel A., 1995, ARA&A, 33, 163
Webb J. R., 2021, Galaxies, 9, 69
Webb J. R. et al., 2021, Galaxies, 9, 114
Zhang X. H., Bao G., 1991, A&A, 246, 21

APPENDIX: SOME EXTRA MATERIAL

Table A1. The sample of 53 blazars used in our study.

Target Id	SDSS name	RA (J2000) (deg)	Dec. (J2000) (deg)	Redshift (z)	$m_r{}^a$	Fermi detection and class[b]
1	J054407−224109	86.031 531	−22.686 088	1.54	16.14	–
2	J061038−230145	92.661 609	−23.029 389	2.85	18.52	–
3	J061357+130645	93.490 388	13.1126 23	0.74	18.47	–
4	J063053−132334	97.724 612	−13.392 908	1.02	18.28	–
5	J064828−174405	102.118 740	−17.734 838	1.23	17.26	–
6	J065358+370540	103.492 837	37.094 618	1.98	18.17	–
7	J071044+422054	107.684 692	42.348 643	1.16	18.21	–
8	J071355+193500	108.482 003	19.583 465	0.54	18.68	LSP
9	J071424+353439	108.603 405	35.577 737	1.62	18.22	–
10	J072201+372228	110.505 261	37.374 635	1.63	17.99	–
11	J072516+142513	111.320 038	14.420 509	1.04	18.22	LSP
12	J072614+215320	111.559 419	21.888 938	1.86	18.46	–
13	J073051+404950	112.713 957	40.830 805	2.50	18.50	–
14	J073256+254838	113.234 483	25.810 795	1.44	18.60	–
15	J073807+174219	114.530 811	17.705 291	0.42	17.21	LSP
16	J074110+311200	115.294 601	31.200 086	0.63	16.56	–
17	J074344+232838	115.937 384	23.477 522	0.78	18.58	–
18	J074451+292006	116.214 022	29.335 029	1.18	17.00	–
19	J074559+331334	116.497 199	33.226 175	0.61	17.91	–
20	J074836+240024	117.150 463	24.006 714	0.41	17.87	LSP
21	J075052+123104	117.716 864	12.518 025	0.89	17.04	–
22	J075448+303355	118.703 559	30.565 299	0.80	18.02	–
23	J075650−154205	119.211 253	−15.70 1501	1.42	18.75	–
24	J080018+164556	120.078 301	16.765 915	0.31	18.17	–
25	J081126+014652	122.861 289	1.7811 81	1.15	18.02	LSP
26	J082550+030924	126.459 751	3.156 819	0.51	18.74	LSP
27	J084205+183541	130.521 237	18.594 738	1.27	16.79	–
28	J085317+281350	133.324 298	28.230 585	0.92	18.04	–
29	J085441+575729	133.674 992	57.958 341	1.32	17.49	–
30	J085448+200630	133.703 651	20.108 531	0.31	15.09	LSP
31	J090910+012135	137.292 055	1.359 905	1.02	17.07	LSP
32	J090924+521632	137.352 847	52.275 750	0.41	17.68	–
33	J091147+334916	137.949 012	33.821 361	0.46	18.71	HSP
34	J092058+444153	140.243 586	44.698 345	2.19	17.83	LSP
35	J092223−052907	140.598 640	−5.485 319	0.97	17.45	LSP
36	J092507+001913	141.282 581	0.320 545	1.72	17.15	–
37	J092824+444604	142.100 609	44.768 022	1.90	18.32	–
38	J093035+464408	142.646 174	46.735 759	2.03	18.53	–
39	J093309+461535	143.288 817	46.259 857	0.78	18.42	–
40	J095227+504850	148.113 797	50.814 097	1.09	17.68	–
41	J095738+552257	149.409 102	55.382 734	0.90	17.28	LSP
42	J100724+580203	151.853 701	58.034 324	3.35	17.49	–
43	J100811+470521	152.047 613	47.089 325	0.34	18.42	–
44	J104146+523328	160.444 922	52.557 857	0.68	17.04	–
45	J104703−130832	161.766 388	−13.14 2327	1.29	17.21	–
46	J183243+135747	278.179 821	13.963 350	2.83	17.23	–
47	J185027+282513	282.614 955	28.420 337	2.54	17.49	–
48	J191810+552038	289.544 790	55.344 070	1.73	18.84	–
49	J193653−040245	294.223 937	−4.045 945	0.49	18.66	–
50	J195542+513148	298.928 072	51.530 154	1.21	18.08	LSP
51	J202456+171813	306.235 685	17.303 681	1.05	17.83	–
52	J203147+545503	307.949 834	54.917 550	1.26	17.07	–
53	J235342+551840	358.426 244	55.311 306	1.93	18.47	–

Notes. [a]Median magnitude over the ZTF/INOV session.$\nu_s^{peak} < 10^{14}$ Hz).

[b]LSP: low synchrotron peaked BL (i.e. $\nu_s^{peak} < 10^{14}$ Hz), HSP: high synchrotron peaked BL (i.e. $\nu_s^{peak} > 10^{16}$ Hz) (Abdo et al. 2010).

Table A2. The sample of 132 RQQs used in our study.

Target Id	SDSS name	RA (J2000) (deg)	Dec. (J2000) (deg)	Redshift z	$m_r{}^a$
1	J032108+413220	50.285 212	41.539 155	2.47	17.12
2	J072517+434553	111.323 039	43.764 857	1.59	17.53
3	J073330+370818	113.378 585	37.138 522	1.14	18.09
4	J074125+435605	115.354 670	43.934 930	0.66	17.91
5	J074224+342847	115.604 057	34.480 018	1.00	18.28
6	J074358+323512	115.992 811	32.586 832	0.91	17.25
7	J074420+381839	116.086 562	38.311 087	0.41	17.81
8	J074445+200014	116.190 399	20.004 137	1.72	17.03
9	J074451+292006	116.214 022	29.335 029	1.18	16.92
10	J074458+301849	116.243 619	30.313 655	0.58	17.90
11	J074511+191942	116.296 970	19.328 622	0.38	18.17
12	J074527+222453	116.364 277	22.414 816	1.35	17.30
13	J074601+255635	116.507 260	25.943 216	0.68	17.91
14	J074645+314149	116.687 709	31.697 041	0.33	17.86
15	J074820+340752	117.087 376	34.131 323	0.34	18.15
16	J075054+425219	117.727 694	42.872 028	1.91	16.19
17	J075222+273823	118.095 486	27.639 782	1.06	17.06
18	J075251+181108	118.212 981	18.185 625	1.92	18.17
19	J075331+182117	118.382 698	18.354 798	1.83	18.71
20	J075524+342134	118.850 456	34.359 598	2.12	17.80
21	J075545+142941	118.941 219	14.494 748	0.54	18.04
22	J075851+220457	119.714 674	22.082 731	0.82	16.98
23	J080112+191544	120.302 700	19.262 468	0.41	16.73
24	J080141+124208	120.423 193	12.702 425	1.36	18.75
25	J080148+174316	120.453 578	17.721 203	0.42	18.67
26	J080320+252602	120.833 697	25.434 016	0.48	17.68
27	J080356+365723	120.986 896	36.956 654	1.23	18.02
28	J080630+144242	121.626 243	14.711 801	1.22	16.94
29	J080704+360353	121.770 407	36.064 887	0.47	17.69
30	J080954+074355	122.476 615	7.732 000	0.65	16.61
31	J081014+204021	122.560 971	20.672 652	2.52	17.33
32	J081331+254503	123.380 356	25.750 871	1.51	16.08
33	J081558+154055	123.993 161	15.682 035	2.23	17.72
34	J082234+170935	125.643 085	17.160 016	1.78	18.84
35	J082443+201901	126.182 536	20.317 028	0.54	18.75
36	J083103+214553	127.765 630	21.764 860	1.53	18.60
37	J084912+144754	132.302 033	14.798 563	0.86	18.04
38	J084952+363927	132.469 769	36.657 773	1.22	17.51
39	J085435+311020	133.649 394	31.172 445	0.85	17.27
40	J085502+321730	133.761 865	32.291 824	1.11	17.53
41	J085507+110139	133.779 817	11.027 697	1.07	18.28
42	J085903+123903	134.764 826	12.651 006	1.21	17.60
43	J085648+141321	134.202 769	14.222 786	0.34	17.69
44	J085733+160017	134.388 345	16.004 941	0.83	17.27
45	J085813+203746	134.555 582	20.629 494	0.79	17.48
46	J085831+554922	134.630 476	55.822 876	2.06	17.70
47	J085853+063909	134.722 608	6.652 667	1.89	18.47
48	J085924+463717	134.851 446	46.621 488	0.92	16.99
49	J090014+232109	135.058 991	23.352 713	1.42	18.60
50	J090026+204158	135.110 491	20.699 672	0.71	17.91
51	J090219+233534	135.581 513	23.593 048	1.30	18.07
52	J090450+230118	136.209 173	23.021 895	0.48	17.88
53	J090508+074151	136.286 912	7.697 576	2.04	17.72
54	J090529+253033	136.371 561	25.509 275	0.82	18.47
55	J090607+030036	136.531 985	3.010 051	1.68	18.22
56	J090824+033929	137.100 603	3.658 321	1.26	16.89
57	J090832+102152	137.135 897	10.364 733	0.79	17.19
58	J090850+254447	137.210 097	25.746 396	0.45	17.96
59	J090903+473716	137.263 959	47.621 156	1.04	17.48
60	J090906+323630	137.275 758	32.608 415	0.81	17.02
61	J090916+163522	137.317 023	16.589 605	1.07	17.47
62	J091120+172231	137.836 808	17.375 582	0.65	17.91
63	J091135+293803	137.895 866	29.634 379	0.61	17.90
64	J091145+145556	137.937 671	14.932 477	1.27	17.17

Table A2 *– continued*

Target Id	SDSS name	RA (J2000) (deg)	Dec. (J2000) (deg)	Redshift z	$m_r{}^a$
65	J091213+513210	138.057 214	51.536 264	1.48	18.75
66	J091307+442014	138.282 660	44.337 322	2.93	18.51
67	J091334+352540	138.395 716	35.428 052	2.16	17.85
68	J091431+083742	138.632 417	8.628 568	0.65	17.08
69	J091511+201248	138.795 985	20.213 429	1.24	17.15
70	J091624+040943	139.103 242	4.162 055	0.31	17.81
71	J091755+053749	139.479 292	5.630 493	0.35	18.19
72	J091811+524255	139.545 982	52.715 538	2.11	17.89
73	J091845+060226	139.691 350	6.040 617	0.79	17.51
74	J091938+360246	139.911 014	36.046 415	0.60	17.90
75	J092011+495403	140.047 255	49.901 111	1.69	17.12
76	J092100+183605	140.251 579	18.601 638	1.24	17.69
77	J092234+204020	140.644 077	20.672 439	0.94	18.04
78	J092311+450918	140.796 077	45.155 261	1.11	18.03
79	J092537+102115	141.406 856	10.354 286	1.15	17.55
80	J092635+044013	141.646 336	4.670 418	1.43	17.61
81	J092658+093248	141.745 314	9.546 807	0.42	17.97
82	J092702+084758	141.760 914	8.799 665	2.20	17.88
83	J092703+522316	141.763 298	52.387 948	0.60	16.74
84	J092712+124458	141.801 348	12.749 728	1.28	17.00
85	J092727−020833	141.864 283	-2.142 488	0.77	18.57
86	J092756+253007	141.987 012	25.502 194	1.20	16.83
87	J093015+482830	142.564 691	48.475 261	0.50	18.76
88	J093021+235329	142.591 111	23.891 627	1.17	17.12
89	J093046+031326	142.693 573	3.224 156	1.48	17.62
90	J093048+230637	142.703 793	23.110 538	0.47	18.68
91	J093113+052421	142.806 463	5.406 035	1.25	17.34
92	J093131+100337	142.879 506	10.060 509	0.80	18.47
93	J093210+501028	143.045 254	50.174 574	0.51	17.96
94	J093244+500938	143.184 913	50.160 668	0.84	18.47
95	J093518+020415	143.825 816	2.071 010	0.65	16.99
96	J093520+335548	143.836 138	33.930 054	0.69	17.91
97	J093531+451927	143.882 227	45.324 364	0.67	18.98
98	J093623+171726	144.099 697	17.290 848	0.50	18.76
99	J093651+104611	144.213 051	10.769 878	2.77	18.55
100	J093759+453801	144.498 376	45.633 888	0.43	18.75
101	J093809+450420	144.539 700	45.072 382	1.55	17.51
102	J093826+192935	144.608 604	19.493 153	0.40	18.03
103	J093833+225031	144.641 444	22.842 134	0.43	17.69
104	J094202+042244	145.508 538	4.379 059	3.27	17.40
105	J094323+020411	145.847 240	2.069 836	0.95	18.14
106	J094404+480646	146.018 439	48.112 955	0.39	18.17
107	J094526+083629	146.361 811	8.608 149	1.46	18.75
108	J094607+495412	146.530 444	49.903 581	0.76	17.48
109	J094617+135425	146.574 110	13.907 049	1.85	18.71
110	J094651+494703	146.713 263	49.784 333	0.99	18.05
111	J094754+223752	146.975 601	22.631 240	2.54	18.58
112	J095047+480047	147.697 857	48.013 174	1.74	17.17
113	J095122+223144	147.843 926	22.528 937	2.22	17.86
114	J095216+204316	148.068 856	20.721 302	1.43	17.25
115	J095411+561655	148.549 958	56.282 195	2.10	17.79
116	J095714+544017	149.311 138	54.671 553	2.59	17.43
117	J095852+465028	149.717 062	46.841 349	1.16	18.02
118	J095856+570820	149.734 265	57.138 970	1.45	18.75
119	J100114+470232	150.309 700	47.042 271	2.17	17.72
120	J100133+570839	150.391 110	57.144 226	1.37	17.29
121	J100336+460550	150.902 763	46.097 445	1.66	17.99
122	J100502+465927	151.259 788	46.990 950	0.95	17.09
123	J100755+452824	151.982 807	45.473 522	1.65	18.08
124	J101330+531559	153.375 730	53.266 567	1.51	16.31
125	J101719+441704	154.330 649	44.284 505	0.39	17.81
126	J102349+522151	155.955 783	52.364 246	0.96	17.00
127	J103430+470820	158.627 206	47.138 934	0.78	18.03

Table A2 – *continued*

Target Id	SDSS name	RA (J2000) (deg)	Dec. (J2000) (deg)	Redshift z	$m_r{}^a$
128	J104157+473329	160.491 437	47.558 253	1.64	17.26
129	J104336+494707	160.903 063	49.785 466	2.19	17.78
130	J104621+483322	161.589 891	48.556 317	1.58	18.22
131	J105043+500329	162.683 299	50.058 170	0.62	17.51
132	J105141+523934	162.922 480	52.659 525	0.98	18.28

Note. ^{a}Median magnitude over the ZTF/INOV session.
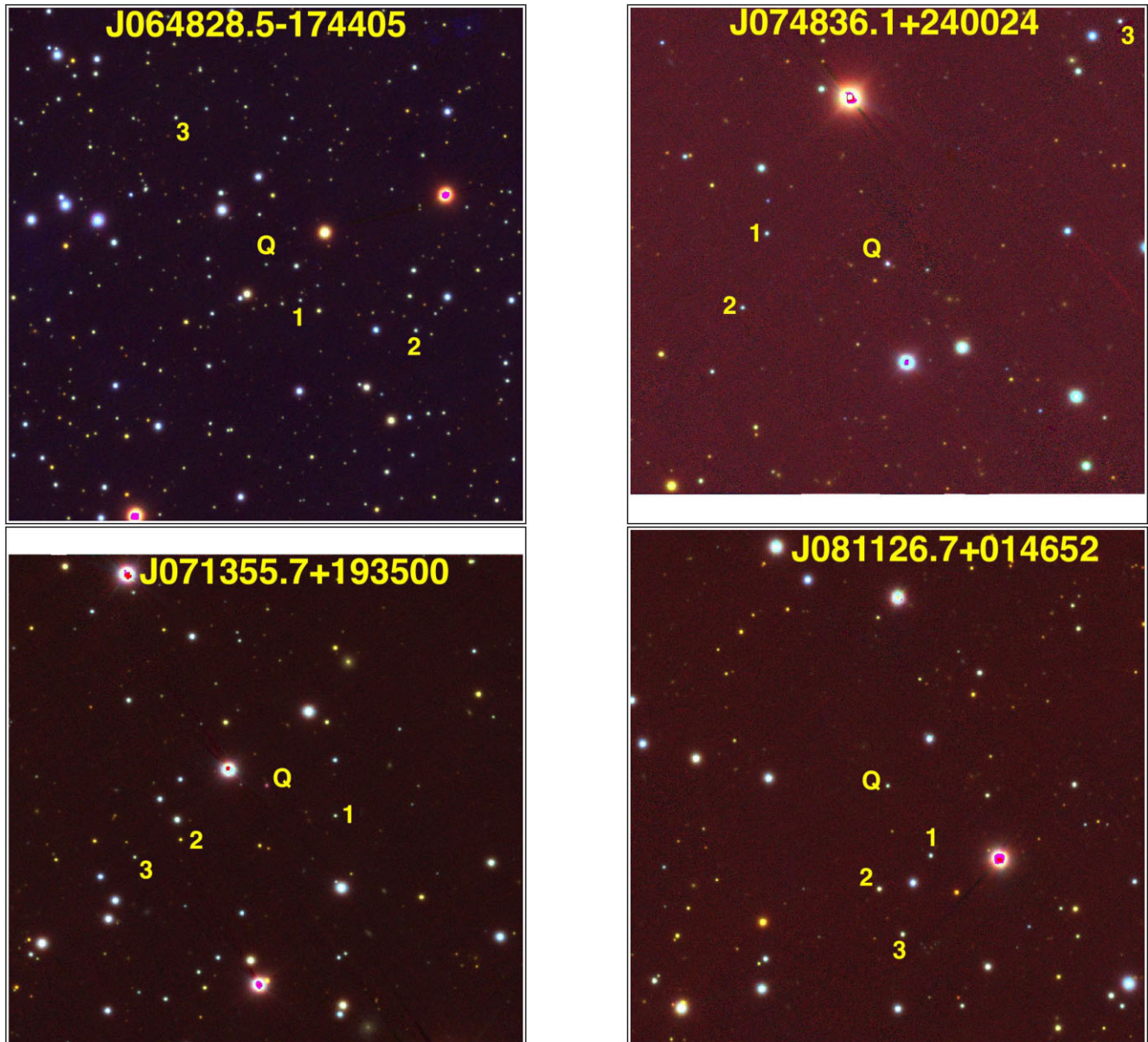
Figure A1. The 5 arcmin × 5 arcmin optical cut-outs of the fields around the four blazars with INOV detection (this work). These cut-outs have been taken from the Panstarrs survey (Chambers et al. 2016). The target blazar and the selected comparison stars are marked with Q, 1, 2, and 3, respectively.
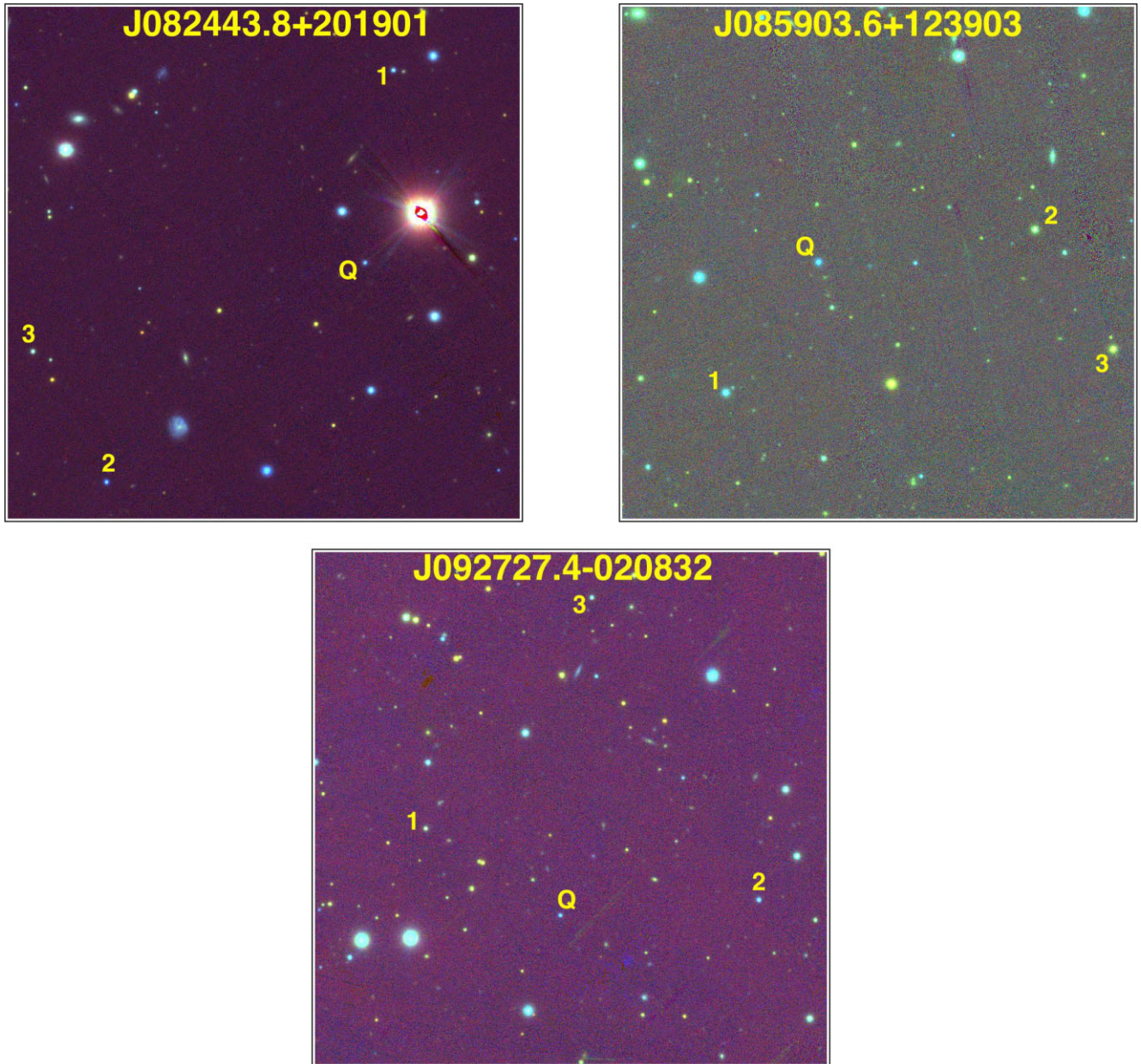
Figure A2. The 5 arcmin × 5 arcmin optical cut-outs of the fields around the three RQQs wih INOV detection (this work). These cut-outs have been taken from the Panstarrs survey (Chambers et al. 2016). The target RQQ and the selected comparison stars are marked with Q, 1, 2, and 3, respectively.

This paper has been typeset from a TEX/LATEX file prepared by the author.